Not just a protein machine: how ribosomes regulate immune response

Dopler-Zandavalle, A.

Chapter 5

Loss of ribosomal protein uL14 enables tumor escape from T cell immunosurveillance

Anna Dopler, Edwin Kyei-Baffour, Mandy Kerkhoff, Ferhat Alkan, Yuval Malka, Kelly Hoefakker, Rob van der Kammen, Liesbeth Hoekman, Onno Bleijerveld, Antonia Bradaric, Maarten Altelaar, Jonathan W. Yewdell, Pia Kvistborg, William James Faller

NAR Cancer, 2025
https://doi.org/10.1093/narcan/zcaf024

Abstract

The presentation of peptides on HLA molecules is essential to CD8+ T cell responses. Here, we show that loss of uL14 significantly downregulates the expression of antigen processing and presentation (APP) components in melanoma cell lines. Peptides generated following knockdown show different characteristics, with altered peptide charge, and differences in anchor residue positions. These peptides also have lower predicted binding to the HLA alleles and a shorter predicted HLA-peptide complex half-life. These result in a functional difference in APP, and knockdown of uL14 causes a reduction in the ability of CD8+ T cells to recognize and kill melanoma cells in a co-culture assay. Together, our data suggest that loss of uL14 alters the peptide pool available for presentation and thus may act as an escape mechanism from tumor immune surveillance.

Graphical Abstract

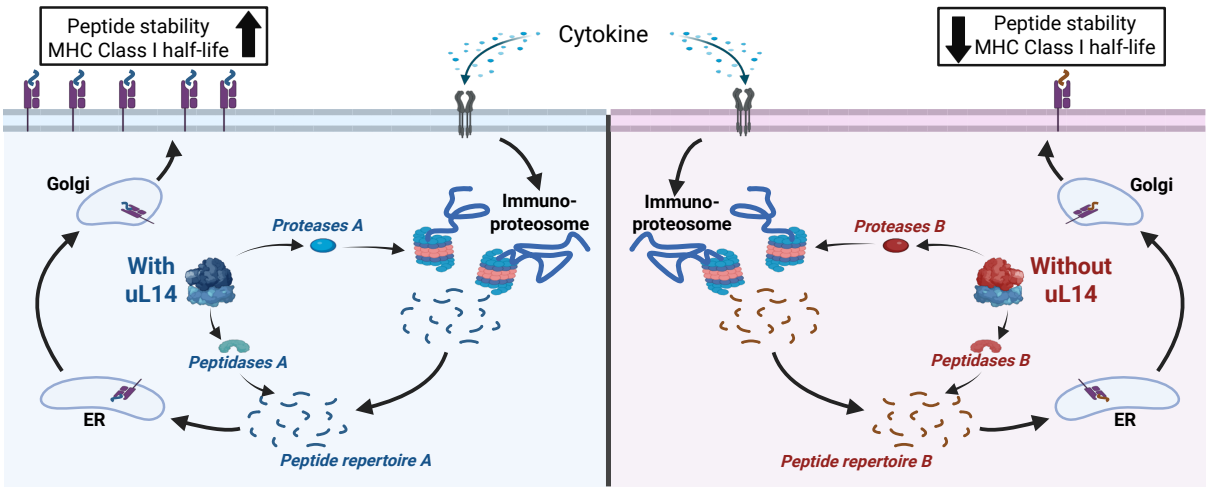

Introduction

Tumor antigenicity is essential for effective CD8+ T cell antitumor immunity [1]. Tumors have myriad immunoevasion strategies, including downregulating antigen processing and presentation machinery (APP) components and alterations to the cancer immunopeptidome, the repertoire of peptides presented to major histocompatibility complex class I molecules (MHC-I) [2–4]. This has been particularly relevant for immune-checkpoint blockade (ICB) therapy approaches, which are based on CD8+ T cell-dependent tumor destruction [5]. While ICB has been incredibly successful in the past years, many patients do not respond or acquire resistance [6].

Despite the importance of T cell-mediated tumor control, it is often unclear how tumor cells escape T cell immunity. While it is clear that downregulating APP often plays a central role, much remains to be learned about how this process is regulated.

Peptide presentation requires the translation of source proteins by ribosomes. Peptides can be generated from either “retirees,” native proteins degraded with a characteristic half-life, or defective ribosomal products (DRiPs), a subset of synthesized proteins that is rapidly degraded due to defects in converting genetic information into native proteins [7, 8]. The “immunoribosome” hypothesis posits that specialized ribosomes generate DRiPs to enhance immunosurveillance [9]. Such ribosomes can potentially arise from variations in either the ribosomal RNA (rRNA) or protein content of the ribosome [10]. Ribosomes have 80 standard ribosomal proteins (RPs), and many RPs are known to be present in sub-stoichiometric amounts [11, 12]. It has been shown that decreasing individual RP expression can alter the immunopeptidome [13], and we have previously found that the translation of APP components is very sensitive to the presence of the ribosomal P-stalk [14].

It has long been known that cancers can escape immunosurveillance by mutating APP component genes, the first example of which was beta-2-microglobulin (β2M) [15, 16]. Alterations in RP genes are common in cancers [10, 17], and it has been shown that RP knockdown can increase presentation of a cancer-specific peptide to CD8+ T cells [13]. In fitting with a role for immunoribosomes in immune response, the RP uL14 (RPL23) was identified among the most essential genes for melanoma resistance to T cell-mediated killing [18]. uL14 was also found to be downregulated in patients with diminished immunological response to antiretroviral therapy against HIV [19]. While uL14 is known to play a crucial role in cell proliferation and apoptosis [20, 21], its role in immunosurveillance is unexplored.

Here, we assess the participation of uL14 in T cell-mediated immune surveillance via the regulation of the APP or alterations in the generated peptide repertoire.

Results and discussion

uL14 KD alters HLA I expression

CRISPR knockout screening implicated uL14 as enabling human melanoma escape from $CD8^+$ T cell killing [18]. Based on our finding that ribosomes can regulate APP via cytokine (IFNγ, TNFα) mediated increase of the P-stalk [14], we first examined the effect of these cytokines on uL14. We failed to detect alterations in uL14 levels in ribosomes of melanoma cells treated with both cytokines (Fig. 1A), suggesting that uL14 incorporation is not a direct response to cytokine exposure.

Using two human melanoma cell lines (Mel624 and M026), we next used three independent lentivirus-encoded shRNAs to knockdown (KD) uL14 (shL14#1, shL14#2, shL14#3), with two scrambled negative controls (shScr#1, shScr#2) and an shRNA targeting a different large subunit RP (shL28). This RP was included as a control as it is present in the same subunit as uL14, and we have previously shown that it does not affect APP. Transduction efficiency (using lentivirus-encoded mCherry (%) expression) was ~80% in the Mel624 cell line and 60%–75% in the M026 cell line (Fig. 1Band Supplementary Fig. S1A), and uL14 KD efficiency [measured by RT-qPCR quantitation of uL14 messenger RNA (mRNA) and immunoblotting uL14 in total cell lysates] was between 29% and 35% for shL23#1, #2, and #3 in the Mel624 cell line, and a 31%–40% KD in the M026 cell line (Fig. 1C and D, and Supplementary Fig. S1B and C).

As a highly conserved RP, uL14 is obviously important for protein synthesis, regulation of which plays a key role in mounting efficient immune responses, especially in the context of APP [36]. We first confirmed that uL14 KD impacts uL14 incorporation in the ribosomes. This showed that uL14 was decreased in the polysomes compared to another large ribosomal subunit protein (uL7), suggesting that intact ribosomes that contain uL7 and not uL14 exist in the cell following KD (Supplementary Fig. S1D and E). Interestingly, uL14 KD only caused a 0%–30% reduction in total protein synthesis measured by incorporation of ^{35}S-methionine (Fig. 1E and Supplementary Fig. S1F), supporting the idea that uL14 KD alters ribosome

composition but does not significantly inhibit ribosome function. It must be highlighted, however, that we do not know the relative contribution of uL14 positive versus uL14 negative ribosomes to translation in this context.

Despite these modest effects, we confirmed that uL14 KD compromises proliferation as previously reported [37] (Fig. 1F and Supplementary Fig. S1G). We next measured total levels of HLA I in uL14 KD cells via immunoblotting, and this showed that uL14 KD decreased HLA I levels in both cell lines (Fig. 1G and Supplementary Fig. S1H). Although protein synthesis in general is decreasing (Fig. 1E), the effect appears to be amplified on HLA I, compared to the loading control.

Figure 1

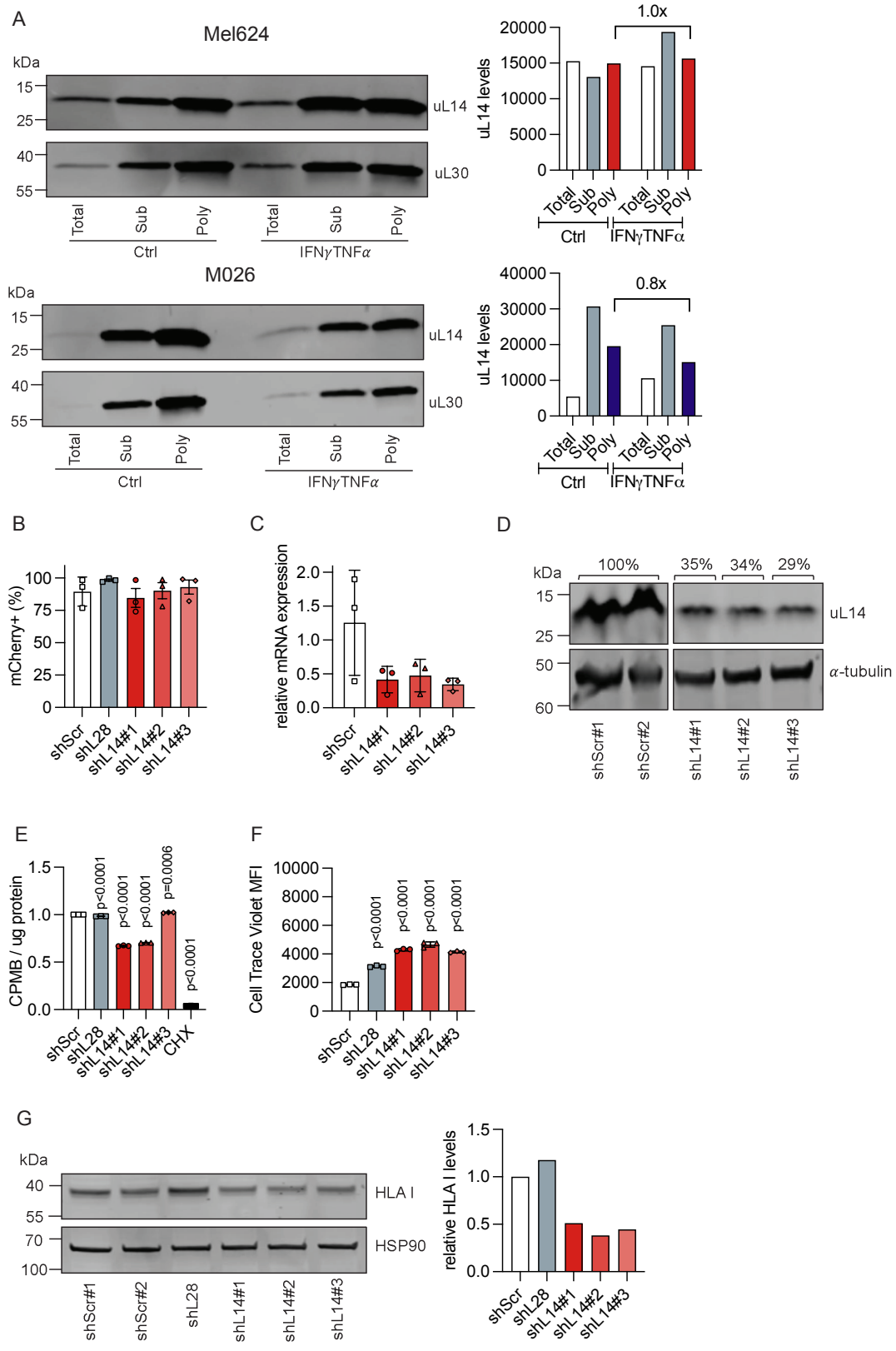

Figure 1. [legend on the next page]

Figure 1 [previous page]. uL14 KD alters protein expression

(**A**) uL14 association with translating ribosomes (poly) is unaltered in Mel624 and M026 tumor cells treated with IFNγ/TNFα compared to untreated cells. uL30 was used as a control for data normalization. *n* = 1 experiment per cell line. uL14 and uL30 expression was additionally assessed in the total protein fraction (total) and the sub-polysomal fraction (sub).

(**B**) Transduction efficiency (measured by % of cells with mCherry expression) of Mel624 cells was measured by flow cytometry gated on live cells. *n* = 3 independent experiments each assessed in triplicates represented as mean ± SEM.

(**C**) RT-qPCR analysis confirming efficient uL14 KD in Mel624 tumor cells. *ACTB* was used as a reference. *n* = 3 technical replicates represented as mean ± SD. *P*-values were calculated using a two-tailed *t*-test.

(**D**) Western blot analysis confirming efficient uL14 KD in Mel624 tumor cells. α-Tubulin was used as loading control. *n* = 1 experiment per cell line.

(**E**) ^{35}S-methionine incorporation assay showing decreased protein synthesis in shL14 Mel624 tumor cells compared to the control. Cycloheximide was used as a control to inhibit protein synthesis. *n* = 3 technical replicates represented as mean ± SD. *P*-values were calculated using a two-tailed *t*-test.

(**F**) CellTrace violet cell proliferation assay showing decreased cell proliferation in shL14 Mel624 cells compared to the control. Proliferation was assessed by flow cytometry using the MFI. *n* = 3 biological replicates represented as mean ± SEM. *P*-values were calculated using a two-tailed *t*-test.

(**G**) Western blot showing decreased HLA I protein levels in shL14 Mel624 tumor cells compared to the control. HSP90 was used as loading control. *n* = 1 independent experiment

uL14 KD is associated with a decrease in MHC I surface presentation

To more broadly understand the effect of uL14 KD in tumor cells, we performed proteomic analysis of both cell lines expressing either shL14 or shScr. Although there was some variability between cell lines, these data revealed that multiple APP components were strongly reduced following KD of uL14, with this being particularly evident in the Mel624 cell line. In this line, HLA-A, HLA-B, HLA-C, HLA-E, β2m, and TAPBP were all significantly reduced (Fig. 2A and Supplementary Fig. S2A). Interestingly, however, in Mel624 uL14 KD cells, two of the three catalytic components of the immunoproteasome (PSMB8 and PSMB9) and several peptidases (BLMH, NPEPPS, and PEPD) increased in abundance following uL14 KD. This suggests that overall peptide presentation may decreased by diminished levels of MHC I and the immunopeptidome may be altered by changes in proteases that liberate and trim peptides (Fig. 2A and Supplementary Fig. S2A).

We repeated this proteomic analysis with tumor cells treated with IFNγ/TNFα. As before, there was substantial cell line-dependent variability; however, contrary to what we found at basal state, uL14 did not interfere with cytokine upregulation of most APP components in the more responsive Mel624 line (Fig. 2A and Supplementary Fig. S2A).

To characterize class I presentation, we measured HLA cell surface levels by flow cytometry using a pan class I and an HLA-A2-specific mAb. As predicted, this revealed that uL14 KD causes a substantial reduction of HLA I surface levels, particularly HLA-A2, in the absence of cytokine exposure (Fig. 2B and Supplementary Fig. S2B). We performed the same experiment after exposing cells to IFNγ/TNFα. Intriguingly, in contrast to the proteomic data (Fig. 2A), cells showed greatly impaired cell surface HLA I levels compared to scrambled control (Fig. 2C and Supplementary Fig. S2C). The discrepancy in total versus cell surface class I suggests that uL14 KD sufficiently compromises peptide generation to limit MHC I surface expression [33, 38, 39].

Figure 2

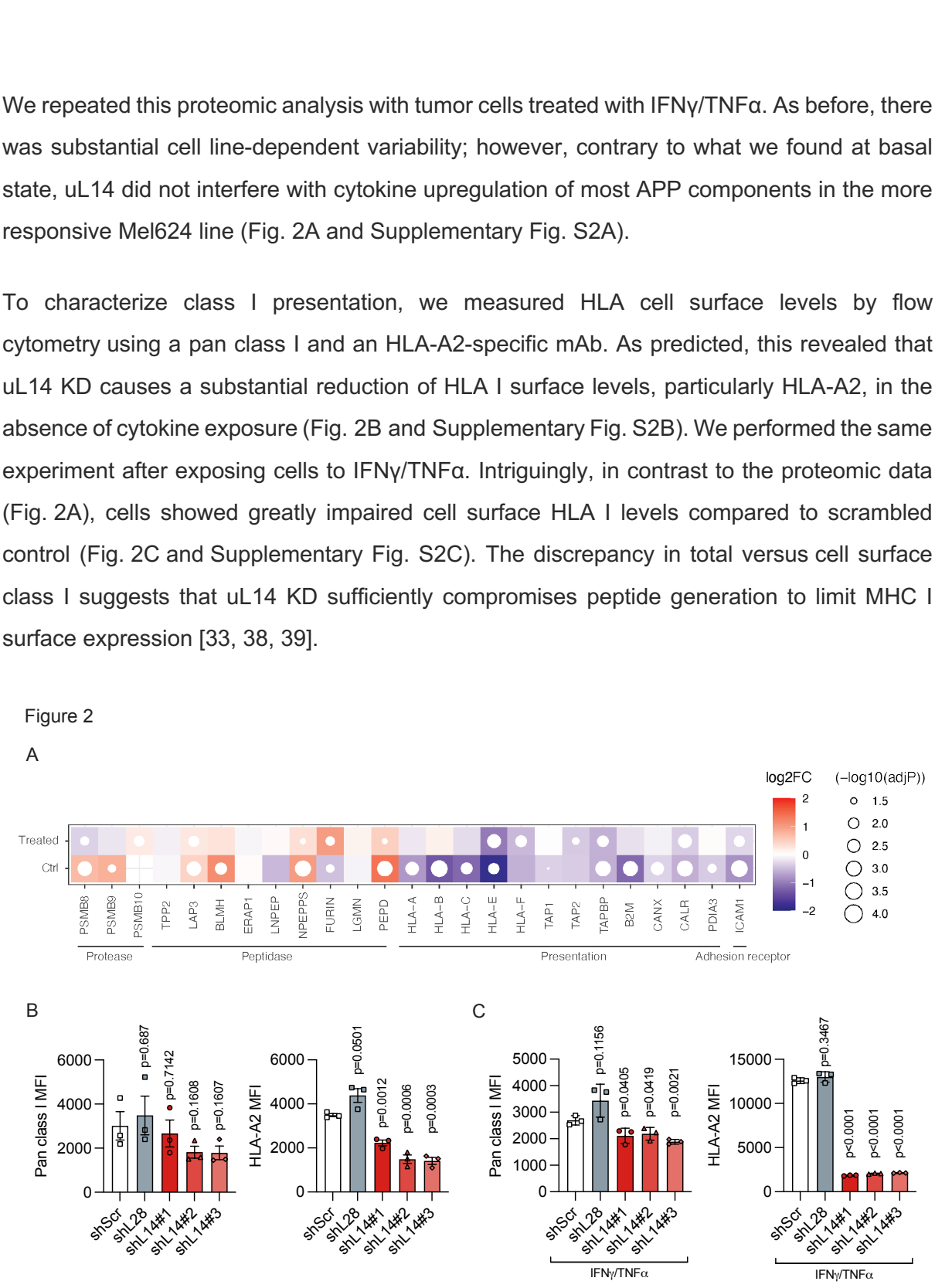

Figure 2. uL14 KD regulates antigen presentation

(**A**) Proteomics analysis of Mel624 cells reveals altered protein levels upon uL14 KD in untreated (Ctrl) cells and cells treated with IFNγ/TNFα (Treated). *n* = 3 independent experiments, and *P*-values were calculated using a two-tailed *t*-test.

(**B**) uL14 KD decreases HLA I surface levels in Mel624 tumor cells. HLA surface levels were measured by flow cytometry using the MFI. *n* = 3 independent experiments each assessed in triplicates. Data are represented as mean ± SEM, and *P*-values were calculated using a two-tailed *t*-test.
(**C**) uL14 KD results in low basal HLA I surface levels in Mel624 tumor cells treated with IFNγ/TNFα compared to the control. *n* = 3 independent experiments each assessed in triplicates. Data are represented as mean ± SEM, and *P*-values were calculated using a two-tailed *t*-test.

uL14 knockdown alters the presented immunopeptidome

To investigate the role of uL14 in peptide generation, we performed immunopeptidomics to assess both the relative amounts and the characteristics of peptides presented after uL14 KD in Mel624 tumor cells. This entails collecting MHC I molecules with a bead bound mAb and analyzing eluted oligopeptides via mass spectrometry of HPLC fractions. To confirm the quality of the immunopeptidomics data, we assessed peptide length distribution and the correlation between predicted and observed peptide HPLC retention times. Identified peptides exhibited a high correlation between observed and predicted retention times, and the expected peptide length distribution was observed, with nearly all peptides ranging from 8 to 14 residues, with ~50% of peptides being nonamers (Supplementary Fig. S3A and B).

uL14 KD resulted in a 10% loss in the variety of unique peptides identified (1240 ± 46 versus 1417 ± 7 in scrambled control treated cells) (Fig. 3A). Seventy-nine percent of peptides were shared between conditions. Although MS cannot quantitate absolute peptide abundance, it accurately measures the differential abundance of the same peptide. Peptides that were decreased in abundance or absent on shL14 cells (labeled “Down”) were compared to those that were increased in abundance on shL14 cells or absent on shScr cells (labeled “Up”). This revealed that uL14 KD resulted in significantly more peptides with decreased abundance than increased (335 versus 93) (Fig. 3B), suggesting that overall peptide presentation may be decreased following uL14 KD.

As we hypothesized that this may be a result of a change in the characteristics of peptides generated following uL14 KD, we next analyzed this in the Down and Up groups. These data showed that the peptides in the Down group were less positively charged than those in the Up group (Fig. 3C) and had changes in their anchor residues (Fig. 3D). Further analysis showed that peptides in the Down group had significantly lower predicted binding affinity to Mel624-specific HLA alleles (Fig. 3E), and a lower predicted peptide–MHC complex half-life (Fig. 3F). Although this has not been experimentally validated, these data support a model wherein uL14

KD causes a change in the peptidases and proteases expressed in a cell, which in turn results in increased production of peptides with low affinity to the specific MHC alleles expressed. These HLA-peptide complexes have a shorter predicted half-life, likely as a result of decreased stability. As these complexes are less likely to be presented on the cell surface, it may explain the observed decrease in cell surface HLA, despite efficient HLA upregulation following cytokine exposure.

Figure 3

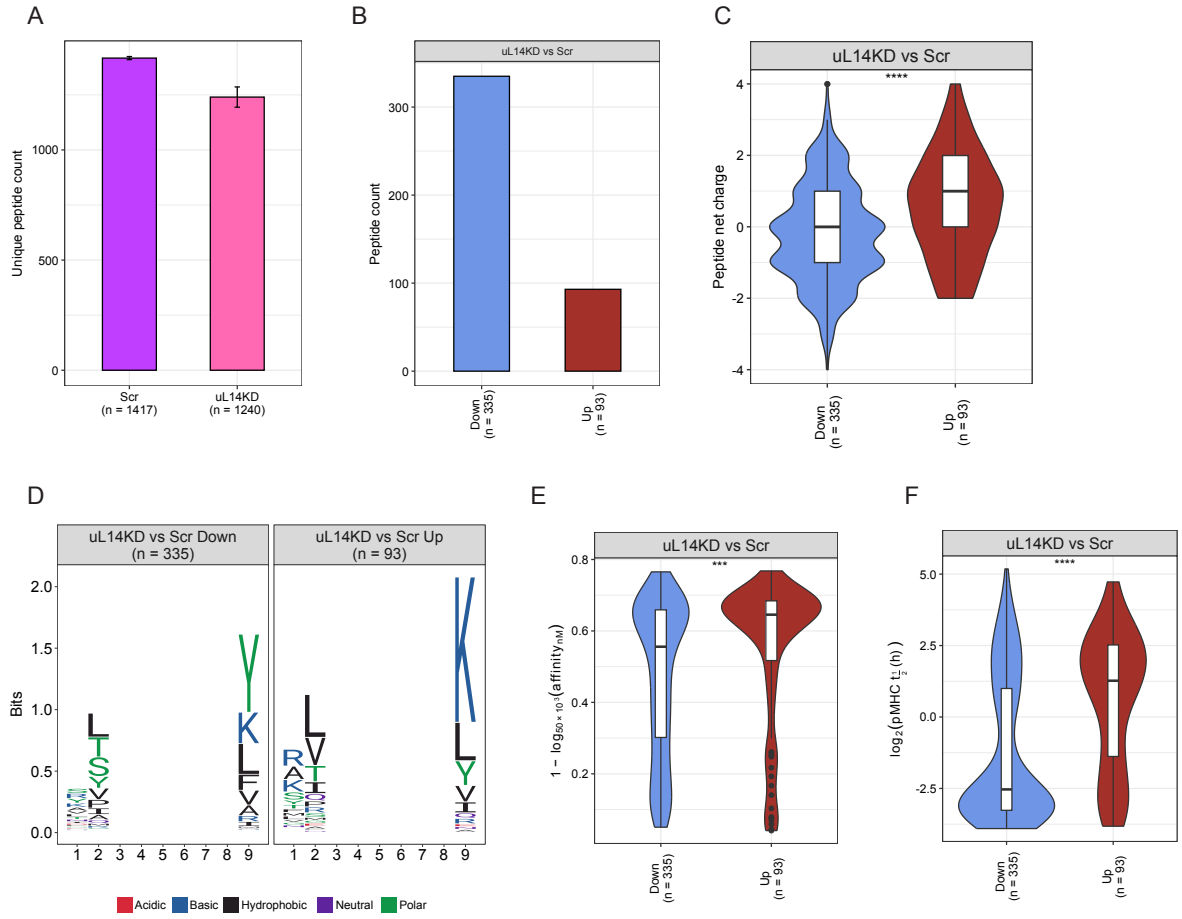

Figure 3. uL14 KD alters the presented peptide pool

(**A**) Immunopeptidomics analysis reveals a decrease in the number of uniquely presented peptides identified in uL14 KD Mel624 tumor cells compared to the shScr control. $n = 2$ independent experiments, and data are represented as mean ± SEM.

(**B**) uL14 KD in Mel624 cells results in high numbers of Down peptides (downregulated compared to the shScr control + peptides exclusively unique to the shScr control) (Down) compared to Up peptides (upregulated compared to the shScr control + peptides exclusively unique to uL14 KD) (Up). Significant peptides were determined using a two-tailed *t*-test without imputation of missing peptides. FDR threshold was set at 0.01 with a dispersion correction factor of 0.1.

(**C**) uL14 KD in Mel624 cells results in a significant increase in net positive charge of Up peptides (upregulated + peptides exclusively unique to uL14 KD). Each violin-boxplot represents the distribution of theoretical net charge of presented Down peptides (downregulated + peptides exclusively unique to the shScr control) and Up peptides (upregulated + peptides exclusively unique to uL14 KD) using the Lehninger pKa scale at a pH of 7.0. *P*-values were calculated using a two-tailed Wilcoxon test (****P < .0001).
(**D**) Peptide N-terminus and anchor residues (position 2 and C-terminus) are altered between Down and Up peptides in shL14 Mel624 cells compared to shScr. Logo plots represent the conservation of amino acid residues at each position and across peptides identified in each group of Down and Up peptides.
(**E**) uL14 KD in Mel624 cells results in significantly lower predicted binding affinity to Mel624-specific HLA alleles in Down peptides compared to Up peptides. Each violin-bar plot represents the distribution of predicted log-transformed affinity (nM) of peptides to HLA alleles A02:01, A03:01, B07:02, B14:01, C07:02, and C08:02. *P*-values were calculated using a two-tailed Wilcoxon test (***P < .001).
(**F**) uL14 KD in Mel624 cells results in significantly lower predicted peptide–MHC (pMHC) complex stability in Down peptides compared to Up peptides. Each violin-bar plot represents the distribution of predicted log-transformed pMHC half-life against Mel624-specific HLA alleles (A02:01, A03:01, B07:02, B14:01, C07:02, and C08:02). *P*-values were calculated using a two-tailed Wilcoxon test (****P < .0001).

uL14 KD impairs CD8$^+$ T cell recognition and killing of tumors

We next tested whether the uL14 KD-induced alteration in peptide processing affects T cell recognition of the MART-1 and NY-ESO-1 antigens on melanoma cells, which may help explain the decrease in cell surface HLA following uL14 KD (Fig. 2B and Supplementary Fig. S2B). For this, we performed a melanoma cell/T cell co-culture assay [13, 18] using CD8$^+$ T cells retrovirally transduced with a TCR specific for HLA-A2 MART-1 or NY-ESO-1 peptide complexes present on Mel624 and M026 tumor cells (Fig. 4A). We measured T cell activation by flow cytometry using three criteria: secretion of IFNγ and TNFα, surface expression of CD107a (Supplementary Fig. S3C), and killing melanoma cells.

uL14 KD in tumor cells significantly decreased the ability of both MART-1- and NY-ESO-1-specific CD8$^+$ T cells to recognize tumor cells, compared to the scrambled controls (Fig. 4B and C, and Supplementary Fig. S4A and B). In line with this, CD8$^+$ T cell killing of tumor cells was significantly impaired following uL14 KD (Fig. 4D and E, and Supplementary Fig. S4C and D). For MART-1, this effect may be largely related to a reduction in MART-1 expression (Fig. 4F and Supplementary Fig. S4E), though we note that shL14#3 KD had the greatest effect on blocking T cell activation and the least effect on reducing MART-1 levels. For NY-ESO-1, there was a clear effect of shL14#1 on T cell recognition along with an increase in NY-ESO-1 (Fig. 4F and Supplementary Fig. S4E), consistent with a selective effect on peptide processing/presentation.

Together, our analysis indicates that uL14 KD alters the peptide pool available for presentation at the level of overall peptide supply and specific peptide generation and provides an explanation for enrichment of uL14 KD cells in the original CRISPR tumor escape study [18].

Figure 4

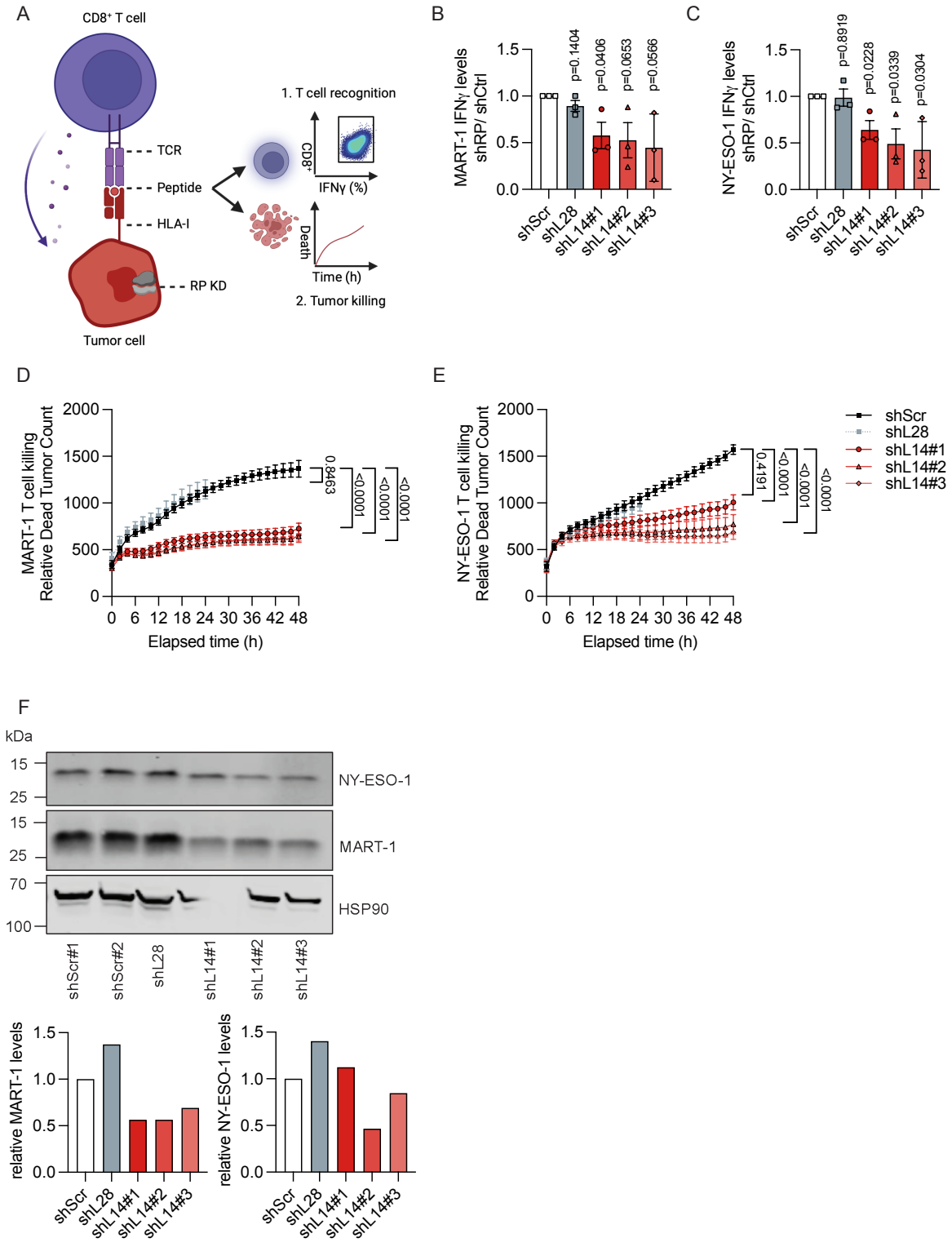

Figure 4. [legend on the next page]

Figure 4 [previous page]. uL14 KD impairs CD8 T cell recognition and killing of tumors.
(**A**) Schematic representation of co-culture and killing assay experiments.
(**B**) MART-1-specific $CD8^+$ T cell recognition (IFNγ levels) is decreased in shL14 Mel624 tumor cells compared to the control. *n* = 3 independent experiments each assessed in triplicates. Data are represented as mean ± SEM, and *P*-values relative to shScrl were calculated using a two-tailed *t*-test.
(**C**) NY-ESO-1-specific $CD8^+$ T cell recognition (IFNγ levels) is decreased in shL14 Mel624 tumor cells compared to the control. *n* = 3 independent experiments each assessed in triplicates. Data are represented as mean ± SEM, and *P*-values relative to shScrl were calculated using a two-tailed *t*-test.
(**D**) MART-1-specific T cell killing is suppressed in shL14 Mel624 tumor cells compared to shScr tumor cells. *n* = 3 independent experiments per cell line, each assessed in triplicates. Data represent mean and error ± SEM, and *P*-values were calculated with a two-tailed *t*-test.
(**E**) NY-ESO-1-specific T cell killing is suppressed in shL14 Mel624 tumor cells compared to shScr tumor cells. *n* = 3 independent experiments per cell line, each assessed in triplicates. Data represent mean and error ± SEM, and *P*-values were calculated with a two-tailed *t*-test.
(**F**) Western blot showing decreased MART-1 and NY-ESO-1 source protein levels in shL14 Mel624 tumor cells compared to the shScr control. HSP90 was used as loading control. *n* = 1 experiment per cell line.

Recent advances in immunotherapy have revolutionized cancer therapy. Checkpoint inhibitor therapy has been approved by the FDA for 20 tumor types. While it can be curative [40], tumor escape remains a major problem [5]. We recently reported a pivotal role for ribosomes in regulating cytokine responses [14], and here we show that other changes to the ribosome have similar, but distinct, impacts on antigen presentation.

As previous work had identified uL14 as a gene product that could alter T cell responses [13, 18], we chose to study this RP in more detail. We have shown that uL14 KD

1. does not greatly reduce protein synthesis;
2. downregulates HLA and other proteins involved in APP at a basal level, but upregulates some proteases and peptidases;
3. does not prevent cytokine-mediated upregulation of APP-related proteins;
4. protects cells from T cell recognition and T cell-mediated killing;
5. alters the characteristics of presented peptides.

In all, these data suggest that uL14 may impact several aspects of APP. KD clearly reduces the levels of many proteins associated with APP; however, the cell is still able to upregulate these proteins following cytokine exposure. Despite this, T cell-mediated killing is still

substantially reduced, which may be explained by changes to the immunopeptidome, suggesting a multifunctional role for uL14 in immune response. In particular, the regulation of enzymes that process antigenic peptides is of note. While several proteins involved in the presentation of antigens are downregulated (including HLA-A, -B, -C, b2M, and Tapasin), we also see an upregulation of proteins involved in processing antigens (PSMB8, PSMB9, BLMH, NPEPPS, and PEPD), suggestive of a difference in the processing of peptides following uL14 KD. Indeed, our analysis of the immunopeptidome appears to bear this out, with clear differences in anchor residues, predicted allele-binding, and resultant MHC:peptide stability. We hypothesize that this may be at least partially behind the decrease in T cell recognition observed after uL14 KD.

This differentiates it from the P-stalk, a component of the ribosome we have previously shown to regulate cytokine responses [14]. The P-stalk is crucial for the translation of transmembrane domains and regulates APP as a result. Interestingly, while KD of P-stalk members does not affect the source proteins of the antigens used in our co-culture assays (MART-1 and NY-ESO-1), uL14 KD does result in a downregulation (Fig. 4F and Supplementary Fig. S4E). This, combined with the change in peptide characteristics after uL14 KD, potentially helps explain why T cell recognition and killing are decreased after uL14 KD. It is also worth pointing out that the ribosome-association of uL14 does not change after cytokine exposure, suggesting that, unlike the P-stalk, it is not part of a cytokine response.

Importantly, we have not shown mechanistically exactly how uL14 regulates these processes. There are a limited number of studies into the function of uL14, but it is known to directly bind eIF6, and as such plays a role in translation initiation [41]. While this role in translation is an obvious mechanism through which uL14 may affect gene regulation, there are also known extra-ribosomal functions, including in the activation of p53, following nucleolar stress [42]. Indeed, TAP1 and ERAP1 (both cytokine-regulated genes) are known to have p53 responsive elements [43, 44], although neither is downregulated following uL14 KD (Fig. 2A and Supplementary Fig. S2A), suggesting that this role of uL14 may not be important in this context.

In all, we have shown that changes to the ribosome can affect APP in different ways. While the P-stalk affects the translation of specific mRNA elements [14], uL14 KD appears to alter the processing of antigens, among other things. It has been hypothesized for decades that ribosomes play a role in regulating APP [7, 9], and the results presented here combined with our previously published study, suggest that this may happen in multiple ways. However, we have not shown whether the regulation of uL14 is a mechanism of resistance to

immunotherapy, nor whether the results presented here are consistent between cell lines/tissues. While our findings suggest ribosomes potentially regulate many aspects of APP, further work needs to be carried out to delineate the precise biological roles.

Acknowledgements

Author contributions: Anna Dopler (Conceptualization [equal], Data curation [lead], Formal analysis [lead], Investigation [lead], Methodology [lead], Writing—original draft [lead], Writing—review & editing [lead]), Edwin Sakyi Kyei-Baffour (Data curation [equal], Formal analysis [equal], Investigation [equal], Methodology [equal], Visualization [equal], Writing—original draft [equal], Writing—review & editing [equal]), Mandy Kerkhoff (Investigation [equal], Methodology [equal]), Ferhat Alkan (Supervision [equal], Visualization [equal], Writing—review & editing [equal]), Yuval Malka (Data curation [equal], Formal analysis [equal], Investigation [equal], Methodology [equal]), Kelly Hoefakker (Methodology [equal]), Rob van der Kammen (Formal analysis [equal], Investigation [equal], Methodology [equal]), Liesbeth Hoekman (Investigation [equal]), Antonia Bradaric (Investigation [equal]), Jonathan W. Yewdell (Resources [equal], Writing—original draft [equal], Writing—review & editing [equal]), Maarten Altelaar (Supervision [equal]), Pia Kvistborg (Conceptualization [equal], Funding acquisition [equal], Resources [equal], Supervision [equal]), and William Faller (Conceptualization [lead], Formal analysis [equal], Funding acquisition [lead], Investigation [equal], Project administration [lead], Resources [lead], Supervision [lead], Writing—original draft [lead], Writing—review & editing [lead]).

Conflict of interest

None declared.

Funding

A.D. and E.K.B. were supported by the Nederlandse Organisatie voor Wetenschappelijk Onderzoek (OCENW-M20-373). A.D. was supported by the Mark Foundation for Cancer Research (21-053-ASP). F.A. and Y.M. were supported by the KWF (13878). Research at the Netherlands Cancer Institute was supported by institutional grants of the KWF and the Dutch Ministry of Health, Welfare and Sport.

Data availability

The proteomics and peptidomics data have been deposited and are publicly available at the PRIDE repository under accession number PRIDE: PXD059093.

Methods

Cell culture

M026 and Mel624 cells were maintained in Dulbecco's modified Eagle medium that was supplemented with 10% fetal bovine serum (FBS) and 100 U/ml penicillin–100 µg/ml streptomycin (Life Technologies, 15140-122). HEK293T cells were maintained in Iscove's modified Dulbecco's medium that was supplemented with 10% fetal calf serum (FCS) and 100 U/ml penicillin–100 µg/ml streptomycin.

Cytokine treatment

Lyophilized cytokines were reconstituted in phosphate buffered saline (PBS) supplemented with 0.1% bovine serum albumin. Cytokine treatment on tumor cells was performed using the combination of human recombinant IFNγ (Peprotech, 300-02; 50 ng/ml) and human recombinant TNFα (Peprotech, 300-01A; 50 ng/ml). Tumor cells were treated for either 24 or 48 h unless stated otherwise.

Patient material

Human peripheral blood mononuclear cells (PBMCs) were isolated from donor buffy coats at the Netherlands Cancer Institute (Amsterdam, The Netherlands). PBMCs were isolated using standard Ficoll gradient centrifugation separation. Isolated PBMCs were either processed fresh or cryopreserved in liquid nitrogen and FBS with 10% dimethyl sulfoxide.

Generation of MART-1- and NY-ESO-1-specific $CD8^+$ T cells

PBMC-derived T cell receptor (TCR)-transduced $CD8^+$ T cells were isolated as described previously [22]. In short, $CD8^+$ T cells were isolated using the human Miltenyi $CD8^+$ T Cell Isolation Kit (Miltenyi Biotec, 130-096-495). Isolated $CD8^+$ T cells were activated using Human T-Activator CD3/CD28 Dynabeads (Miltenyi Biotec, 111.31D) for 48 h at 37°C. For $CD8^+$ T cell TCR transduction, MART-1 or NY-ESO-1 TCR-containing retrovirus was added to a retronectin-coated (Takara, T100A) nontissue culture 24-well plate and mixed with activated $CD8^+$ T cells, spun for 90 min at 2500 rpm at 10°C. After transduction, TCR-transduced $CD8^+$ T cells were harvested and maintained in T cell medium containing Roswell Park Memorial Institute 1640 Medium (RPMI) supplemented with 100 U/ml penicillin–100 µg/ml streptomycin and 10% human serum (HS, Sigma–Aldrich), IL-7 (ImmunoTools, 5 ng/ml), and IL-15 (ImmunoTools, 5 ng/ml). Seven days after transduction, transduction efficiency was measured by flow cytometry with PE a-mouse TCRβ specific antibody (clone H57-597, BD Biosciences, 553172) and anti-PE MicroBeads (Miltenyi Biotec, 130-048-801). Subsequently,

irradiated feeder PBMCs and medium containing 60 U/ml IL-2 (Proleukin, Novartis) and Ultra-LEAF™ Purified anti-human CD3 Antibody (clone OKT3, BioLegend, 317326; 1:2000) were used to rapidly expand successfully transduced MART-1- and NY-ESO-1-specific $CD8^+$ T cells for 5 days. After rapid expansion, $CD8^+$ T cells were expanded for an additional 14 days in medium lacking the Ultra-LEAF™ Purified anti-human CD3 Antibody. Expanded TCR-transduced T cells were either used directly or cryopreserved until needed for an experiment.

Lentivirus shRNAs

All short hairpin RNA (shRNA) targeting sequences used in this study were cloned into a pLV[shRNA]-mCherry:T2A:Puro-U6 > vector purchased from Vectorbuilder. shRNA targeting sequences were selected based on the Broad Institute RNAi Consortium (https://portals.broadinstitute.org/gpp/public/). The used shRNA sequences were: CCTAAGGTTAAGTCGCCCTCG (shScr#1), CAACAAGATGAAGAGCACCAA (shScr#2), CCGCAATTCCTTCCGCTACAA (shL28), CGGTAGGAGCTGTAATCAATT (shL14#1), GCAGGAGTCATAGTGAACAAT (shL14#2), and TGCAGGAGTCATAGTGAACAA (shL14#3). For lentivirus production, HEK293T cells (Sigma–Aldrich, 12022001) were transfected with a second- (pMDL RRE and psPAX2) or third-generation lentiviral packaging system (pVSV-G, pRSV-REV, and pMDLg/RRE). Finally, tumor cells were transduced with shRNA-containing lentivirus at an MOI = 0.5. Transduction efficiency was measured by flow cytometry using mCherry (%) expression 96 h after transduction.

HLA I surface staining

Tumor cells were stained for 30 min with BV605TM anti-HLA-A, -B, -C (clone W6/32, BioLegend, 311432) and APC anti-HLA-A2 (clone BB7.2, BioLegend, 343308), together with LIVE/DEAD Fixable IR Dead Cell Stain Kit (Thermo Fisher, L10199). After staining, cells were washed twice with fluorescence-activated cell sorting (FACS) buffer and measured on the BD FACSymphony™ flow cytometer (BD Biosciences), gated on single and live cells. Data were analyzed using the FlowJo version 10.8.1 software (FlowJo LLC).

CellTrace violet proliferation assay

uL14 knockdown (uL14 KD) and control tumor cells were harvested and washed twice with PBS. After washing, cells were stained for 20 min in the dark with the CellTrace™Violet reagent (Thermo Fisher, C34571; 1:1000) and grown in culture for 96 h after lentiviral transduction. Cell viability was assessed using the LIVE/DEAD Fixable IR Dead Cell Stain Kit (Thermo Fisher, L10199). After staining, cells were washed twice with FACS buffer, and cell proliferation was measured on the BD FACSymphony™ flow cytometer (BD Biosciences),

gated on single and live cells. Data were analyzed using the FlowJo version 10.8.1 software (FlowJo LLC).

^{35}S-methionine incorporation assay

Protein synthesis was measured using a ^{35}S-methionine incorporation assay as described in detail previously [23]. Briefly, 30 µCi/ml ^{35}S-methionine label (Hartmann Analytic, ARS0110) was used to label tumor cells for 120 min at 37°C. After labeling, cells were washed twice with PBS and lysed using lysis buffer (50 mM Tris–HCl, pH 7.5, 150 mM NaCl, 1% Tween A1070320, 0.5% NP-40), protease inhibitor cocktail (Roche, 5892791001), and phosphatase inhibitor cocktail (Sigma, P5726). Whatman filter paper and 25% trichloroacetic acid (TCA) were used to precipitate protein. Precipitated protein was washed twice with 70% ethanol and acetone and scintillation was measured using the liquid scintillation counter (Perkin Elmer). All measured protein amounts were normalized to total protein amounts in each sample.

Immunoblotting

Tumor cell pellets were washed with PBS and lysed with cold lysis buffer [100 mM Hepes, pH 7.5, 300 mM NaCl, 10 mM egtazic acid (EGTA), 3 mM $MgCl_2$, 2% glycerol, 2% Triton X-100 (Sigma)] containing protease inhibitor cocktail (Roche, 5892791001) and phosphatase inhibitor cocktail (Sigma, P5726) for 20 min on ice. Protein was quantified with the Pierce™ BCA Protein Assay Kit (Thermo Scientific, 23227). Equal protein amounts were loaded and separated using ready-to-use 4%–20% Mini-PROTEAN®TGX Stain-Free™ Protein Gels (Biorad, 4568096) and transferred onto 0.2 µm pore nitrocellulose membranes (PALL Life Sciences, 66485). After blotting, membranes were dried for 1 h at room temperature and blocked for 1 h with Intercept (TBS) Blocking Buffer (LI-COR, 927-66003). Blocked membranes were incubated overnight at 4°C with the following primary antibodies: HSP 90α/β (Santa Cruz Animal Health, sc-13119; 1:1000), α-Tubulin (DM1A, Cell Signaling Technology, 3873; 1:1000), RPL23 (Abcam, ab241088; 1:1000), RPL7 (Thermo Scientific, Cat#PA5-36571; 1:1000), MART-1/Melan-A (Thermo Fisher, MS-716-P; 1:1000), NY-ESO-1 (Thermo Scientific, PA5-116201; 1:500), and HLA Class 1 ABC (Abcam, Cat#ab70328; 1:500). After primary antibody incubation, membranes were incubated with the following secondary antibodies for 1 h at room temperature: IRDye® 800CW Goat anti-Rabbit IgG (LI-COR, 926-32211; 1:10000) and IRDye® 680RD Goat anti-Mouse IgG (LI-COR, 926-68070; 1:10000). Images were acquired using the Odyssey CLx (LI-COR) and analyzed with the ImageStudioLite version 5.2.5 (LI-COR) or Empiria Studio version 1.3.0.83 (LI-COR) software.

LC–MS protein quantification

Polysome fractionation and protein precipitation

Ice-cold polysome lysis buffer [10× gradient buffer (1.1 M potassium acetate, 0.2 M magnesium acetate, 0.1 M HEPES, pH 7.6), 100 mM KCl, 10 mM $MgCl_2$, 0.1% NP-40, 154.25 mg/ml Dithiothreitol (DTT), 100 µg/ml cycloheximide (Sigma–Aldrich, C7698), RNaseOUT™ Recombinant Ribonuclease Inhibitor (Thermo Scientific, 10777019), and combined Halt™ Protease and Phosphatase Inhibitor EDTA-free (Thermo Scientific, 78443)] was used to lyse tumor cells for polysome fractionation. Protein lysates were homogenized using a 27G needle and centrifuged for 10 min at 14 000 × *g*. Fifty microliters of the cleared supernatant was collected to measure total protein amounts, while the rest was loaded onto a 10%–60% sucrose gradient. Samples were separated under vacuum at 38 000 rpm for 2 h at 4°C using a Beckman Coulter SW47Ti rotor. Monosome-containing fractions 6–8 (750 µl per fraction), polysome-containing fractions 9–14 (750 µl per fraction), and total protein were collected and protein was extracted following a standard TCA precipitation protocol [24]. Dry protein pellets were either frozen in liquid nitrogen and stored at −80°C or reconstituted in 1× Laemmli Sample Buffer (Biorad, #1610737EDU) for immunoblotting. Total protein pellets were dissolved in 400 µl, monosome-containing pellets in 150 µl, and polysome-containing pellets in 50 µl of 1× Laemmli Sample Buffer. For immunoblotting, protein amounts were quantified using a standard Pierce™ BCA Protein Assay Kit (Thermo Scientific, 23225).

Total protein quantification

Protein was digested from frozen pellets and lysed using boiling guanidine (GuHCl) as described previously [25]. After lysis, a Pierce Coomassie (Bradford) Protein Assay Kit (Thermo Scientific) was used to quantify protein amounts according to manufacturer's instructions. Samples were diluted to 2 M GuHCl and digested at 37°C for 4 h and overnight with trypsin (Sigma–Aldrich) in an enzyme:substrate ratio of 1:75. Formic acid (FA) (1% final concentration) was used to stop digestion and peptides were loaded on the Evotip Pure™ (Evosep). The Evosep One LC system connected to an Orbitrap Exploris 480 Mass Spectrometer (Thermo Scientific) was used to carry out Liquid Chromatography-Tandem Mass Spectrometry (LC–MS/MS) analysis. Peptides were separated on an EV1137 (Evosep) column with an 88-min gradient (extended method) with an EV1086 (Evosep) emitter. The Exploris 480 was set to 120 000 at *m*/*z* 200 with full MS resolution. MS1 mass range was set between 350 and 1400, normalized AGC target was 300%, and maximum IT was 45 ms. Data were acquired in data-independent acquisition (DIA) mode, and DIA was performed on precursors from 400 to 1000 in 48 windows of 13.5 Da with an overlap of 1 Da. Resolution was set to 30 000 and normalized collision energy (CE) was 27.

Data analysis

For total protein quantification, raw data were analyzed without a spectral library using DIA-NN (version 1.8) [26] and the “Deep learning” option enabled. For the library-free search, the SwissProt human database (20 395 entries, release 2021_04 for ribosomal fractions MS; 20 398 entries, release 2022_08 for KD MS) was added. The Robust LC (high accuracy) was used as a quantification strategy, the MBR option was enabled, and all other settings were not changed. Protein group abundances were extracted from DIA-NN result files and imported to Perseus (version 2.0.7.0) [27]. Subsequently, samples were filtered for presence in at least three out of four replicates in one condition. For total protein fractions, *vsn* was performed in the presence of all detected proteins. Statistical significance was determined using a two-sided *t*-test and Benjamini–Hochberg *P*-value adjustment.

RNA isolation and RT-qPCR

The ISOLATE II RNA Mini Kit (BioCat BIO-52072-BL) was used to extract RNA from tumor cell samples, according to manufacturer’s instructions. Isolated RNA was dissolved in nuclease-free water and quantified using the Nanodrop (Thermo Scientific). For reverse transcription, the High-Capacity cDNA Reverse Transcription Kit (Thermo Scientific, 4368814) was used. SYBR^{TM} Green PCR Master Mix (Thermo Fisher, 4367659) was used for quantitative polymerase chain reaction (qPCR). Gene expression was analyzed using the comparative CT method and three technical replicates per sample. Data were normalized to the housekeeping gene ACTB. Primers used for qPCR in this paper were *ACTB* forward (5′-CCTGGCACCCAGCACAAT-3′), *ACTB* reverse (5′-GGGCCGGACTCGTCATACT-3′), *RPL23* forward (5′-GCCAACTGAACAGGCATAAAG-3′), and *RPL23* reverse (5′-CGCTGGGTGTCACCTAAATAA-3′).

Tumor cell:T cell co-culture assay

MART-1- or NY-ESO-1-specific CD8^{+} T cells were thawed for 30 min 1 day prior to the experiment in RPMI containing penicillin–streptomycin, 10% HS, and DNase I (Sigma–Aldrich, 10104159001; 1/1000) and recovered overnight in fresh RPMI medium containing penicillin–streptomycin, 10% HS, IL-7 (5 ng/ml), and IL-15 (5 ng/ml). Co-culture of RP KD tumor cells and MART-1- or NY-ESO-1-specific CD8^{+} T cells was performed for 6 h at 37°C at a T cell:tumor cell ratio of 1:1 and in the presence of GolgiPlug (BD Biosciences, 555029) and GolgiStop (BD Biosciences, 554724). Subsequently, cells were harvested and stained with AF700 anti-CD107a (clone H4A3, BD Biosciences, 561340), BUV anti-CD8 (clone SK1, BD Biosciences, 612889), and the LIVE/DEAD Fixable IR Dead Cell Stain Kit. Prior to intracellular cytokine staining, cells were fixed and permeabilized with the Foxp3 Transcription Factor

Staining Buffer Set (eBioscience, 00-5523-00). Cells were then intracellularly stained with APC anti-IFNγ (clone B27, BD Biosciences, 554702) and FITC anti-TNFα (clone MAb11, BD Biosciences, 554512), and measured the following day with the BD FACSymphony™ flow cytometer (BD Biosciences), gated on single and live $CD8^+$ T cells. Data were analyzed with the FlowJo version 10.8.1 software (FlowJo LLC).

Incucyte killing assay

Similarly to as described above, MART-1- or NY-ESO-1-specific $CD8^+$ T cells were thawed 1 day before the experiment. MART-1- and NY-ESO-1-specific $CD8^+$ T cells and tumor cells were mixed at a ratio of 1:1. Tumor death was measured with the Incucyte Caspase-3/7 Green Dye (Sartorius, 4440; 5 µM). Cells were allowed to settle for 30 min at 37°C after which fluorescent images were captured every 2 h with the Incucyte Live-Cell Analysis System (Sartorius) for 48 h in total. Data were analyzed using dead tumor cell count with the integrated Incucyte Base Analysis Software (Satorius). Importantly, data were normalized to a tumor cell only control to account for tumor cell death independent of T cell killing.

Immunopeptidomics

Sample generation

For immunopeptidomics, 2×10^8 tumor cells per condition were used. Cultured cells were washed with warm PBS and detached using PBS containing UltraPure™ 0.5 M ethylenediaminetetraacetic acid (EDTA), pH 8 (Thermo Scientific, 15575020). Cells were centrifuged for 5 min at 300 × *g*, and cell pellets were resuspended in 10 ml PBS. Cells were again washed with PBS and centrifuged for 5 min at 300 × *g*, and pellets were either frozen in liquid nitrogen and stored at −80°C or lysed directly. Cells were lysed on ice for 1 h in 4 ml PBS lysis buffer containing 0.25% sodium deoxycholate, 0.2 mM iodoacetamide, 1 mM EDTA, 1% octyl-β-D-glucopyranoside, 0.1 mM phenylmethylsulfonyl fluoride, and cOmplete™ Protease Inhibitor Cocktail (Sigma–Aldrich, 11697498001). Lysates were cleared at 4°C for 45 min at 48 000 × *g* and supernatants were collected. For immunoprecipitation, 200 µl of Protein A–Sepharose™ 4B beads (Thermo Scientific, 101042) were used per sample and washed twice with 1 ml lysis buffer at 800 rpm. Washed beads and lysed samples were mixed with 50 µl of W6/32 antibody (10 mg/ml, in-house) and incubated on a rotor at 4°C overnight. On the following day, samples were centrifuged for 5 min at 300 × *g* and beads were washed four times with 1 ml of 150 mM NaCl in 20 mM Tris–HCl (pH 8), twice with 1 ml of 400 mM NaCl in 20 mM Tris–HCl (pH 8), twice with 1 ml of 150 mM NaCl in 20 mM Tris–HCl (pH 8), and finally, four times with 1 ml of 20 mM Tris (pH 8) buffer. As affinity plate, a 96-well single-use microplate with 3-mm glass fiber and 10-mm polypropylene membranes (204495-

100, Agilent) was used and washed with 1 ml of 100% acetonitrile (ACN), followed by 1 ml of 0.1% trifluoroacetic acid (TFA), and then with 2 ml of 0.1 M Tris–HCl (pH 8). For peptide elution, a Sep-Pak tC18 100 mg Sorbent 96-well plate was used and washed with 1 ml of 80% ACN in 0.1% TFA and 2 ml of 0.1% TFA. Air pressure was adjusted to 3–5 psi, and HLA I complexes and bound peptides were eluted with 1% TFA. HLA I peptides were eluted with 28% ACN in 0.1% TFA. Eluted samples were stored at −80°C until submitted for LC–MS/MS analysis.

Data acquisition of HLA peptides by LC–MS/MS

After vacuum drying the IP eluates, peptides were reconstituted in 0.1% formic acid and analyzed by LC–MS/MS on an Orbitrap Exploris 480 Mass spectrometer, connected to an Evosep One LC system (Evosep Biosystems, Denmark). Samples were loaded in their entirety onto Evotip Pure™ (Evosep) tips. Peptides were then eluted on-line and separated using the preprogrammed “Extended Method” (88-min gradient) on an EV1137 (Evosep) column with an EV1086 (Evosep) emitter. Nanospray was achieved using the Easy-Spray NG Ion Source (Thermo Scientific) with a liquid junction setup at 1.6 kV. The Exploris 480 was operated as follows. Application mode was set to “Peptide,” and data-dependent acquisition was performed in Top Speed mode with 1 s. cycle time. Full MS1 scans were acquired at resolution of 60 000 with *m*/*z* 375–1500 mass range. For both MS1 and MS2, AGC target and maximum injection time mode were set to “standard” and “auto,” respectively. Peptides with charge states 2–6 were included for fragmentation; precursors were isolated in the quadrupole with 1.2 *m*/*z* window and subjected to HCD fragmentation with a normalized collision energy of 30%. Fragment ions were detected in the Orbitrap analyzer at 15 000 resolution.

Data analysis

In peptide identification using database searching, the mass spectrometry raw data were analyzed using MaxQuant version 2.0.3.0 [28] as described previously [29]. The raw mass spectrometry data were searched against a combined database of GENCODE Human hg38 version 34 proteome and peptides from noncanonical ORFs from parallel Ribo-seq data. In the search parameters, unspecific enzyme digestion was used with cysteine carbamidomethylation as fixed modification, and methionine oxidation and N-terminal acetylation as variable modification. Peptide matches were to a peptide length of 8–25 amino acids, a maximum mass of 4600 Da, and a maximum precursor and fragment mass deviations of 6 ppm and 20 ppm, respectively. An FDR of 0.01 was used for peptide identification and “match between runs” was allowed for label-free quantification (LFQ) of identified peptides.

MaxQuant peptide output was used to obtain uniquely identified peptides after removing peptide contaminants, reverse peptides, and peptides with zero LFQ across all samples. For quality control of the identified peptides, the correlation of predicted and observed peptide retention times was assessed. Retention times were predicted using chronologer version 0.2.0 (https://github.com/searlelab/chronologer/tree/main). The number of peptides and the distribution of peptide lengths were determined with the majority of peptides expected to have a peptide length of nine amino acids. Peptide length was restricted to 8–15 amino acids to cover both canonical length (8–11 amino acids) and slightly longer peptides that have been reported to occur in the immunopeptidome [30, 31].

For differential analysis of peptides, LFQ intensities were $\log_2$ transformed and width normalized in Perseus version 2.0.11 [27] with no imputation. Differential analysis was performed using a two-sided unpaired *t*-test, comparing uL14 KD to the Scr control at an FDR of 0.01 with a dispersion correction factor of 0.1. Downregulated peptides were combined with peptides restricted to the scrambled (Scr) control to generate the Down group of peptides, and upregulated peptides were combined with peptides restricted to the uL14KD to create the Up group.

The binding affinity of Down and Up peptides to MEL624-specific HLA alleles (A02:01, A03:01, B07:02, B14:01, C07:02, and C08:02) was predicted with MHCflurry version 2.1.2 [32]. The peptides R package version 2.4.6 was used to compute the peptide theoretical net charge, and peptide–MHC binding stability was predicted using netMHCstabpan version 1.0 [33]. The ggseqlogo R package version 0.2.0 [35] was used to generate peptide logos showing the occurrence of amino acids in their N-terminus and anchor residues (second and C-terminus amino acids important in HLA groove binding) in each peptide [34] per sample.

Statistical tests and analysis

All details about statistical tests used in each experiment of this study, including the exact value of *n* and what *n* represents, can be found in the figure legends. All *P*-values are shown for each group, and groups were compared to the scrambled (shScr) or untreated control group. Unless indicated otherwise, statistical significance was defined using a confidence level of 99% and $P < .01$ and was calculated using a two-tailed unpaired *t*-test.

References

1. Blank CU,Haanen JB,Ribas A et al. The “cancer immunogram”.Science 2016;352:658–60.https://doi.org/10.1126/science.aaf2834
2. Seliger B,Maeurer MJ,Ferrone S.Antigen-processing machinery breakdown and tumor growth.Immunol Today 2000;21:455–64. https://doi.org/10.1016/S0167-5699(00)01692-3
3. Cornel AM,Mimpen IL,Nierkens S.MHC class I downregulation in cancer: underlying mechanisms and potential targets for cancer immunotherapy.Cancers 2020;12:1760. https://doi.org/10.3390/cancers12071760
4. Garrido F,Aptsiauri N,Doorduijn EM et al. The urgent need to recover MHC class I in cancers for effective immunotherapy.Curr Opin Immunol 2016;39:44–51. https://doi.org/10.1016/j.coi.2015.12.007
5. Waldman AD,Fritz JM,Lenardo MJ.A guide to cancer immunotherapy: from T cell basic science to clinical practice.NatRev Immunol 2020;20:651–68. https://doi.org/10.1038/s41577-020-0306-5
6. Zhou X,Ni Y,Liang X et al. Mechanisms of tumor resistance to immune checkpoint blockade and combination strategies to overcome resistance.Front Immunol 2022;13:915094. https://doi.org/10.3389/fimmu.2022.915094
7. Yewdell JW,Antón LC,Bennink JR.Defective ribosomal products (DRiPs): a major source of antigenic peptides for MHC class I molecules? J Immunol 1996;157:1823–6. https://doi.org/10.4049/jimmunol.157.5.1823
8. Antón LC,Yewdell JW.Translating DRiPs: MHC class I immunosurveillance of pathogens and tumors.J Leukoc Biol 2014;95:551–62.
9. Yewdell JW,Nicchitta CV.The DRiP hypothesis decennial: support,controversy,refinement and extension.Trends Immunol 2006;27:368–73.https://doi.org/10.1016/j.it.2006.06.008
10. Ramalho S,Dopler A,Faller WJ.Ribosome specialization in cancer: a spotlight on ribosomal proteins.NAR Cancer 2024;6:zcae029.https://doi.org/10.1093/narcan/zcae029
11. Slavov N,Semrau S,Airoldi E et al. Differential stoichiometry among core ribosomal proteins.Cell Rep 2015;13:865–73. https://doi.org/10.1016/j.celrep.2015.09.056
12. Shi Z,Fujii K,Kovary KM et al. Heterogeneous ribosomes preferentially translate distinct subpools of mRNAs genome-wide. Mol Cell 2017;67:71–83. https://doi.org/10.1016/j.molcel.2017.05.021
13. Wei J,Kishton RJ,Angel M et al. Ribosomal proteins regulate MHC class I peptide generation for immunosurveillance.Mol Cell 2019;73:1162–73.https://doi.org/10.1016/j.molcel.2018.12.020
14. Dopler A,Alkan F,Malka Y et al. P-stalk ribosomes act as master regulators of cytokine-mediated processes.Cell 2024;187:6981–93. https://doi.org/10.1016/j.cell.2024.09.039
15. Momburg F,Koch S.Selective loss of beta 2-microglobulin mRNA in human colon carcinoma.J Exp Med 1989;169:309–14. https://doi.org/10.1084/jem.169.1.309
16. Restifo NP,Marincola FM,Kawakami Y et al. Loss of functional beta2-microglobulin in metastatic melanomas from five patients receiving immunotherapy.J Natl Cancer Inst 1996;88:100–8. https://doi.org/10.1093/jnci/88.2.100

17. Guimaraes JC,Zavolan M.Patterns of ribosomal protein expression specify normal and malignant human cells.Genome Biol 2016;17:236.https://doi.org/10.1186/s13059-016-1104-z
18. Patel SJ,Sanjana NE,Kishton RJ et al. Identification of essential genes for cancer immunotherapy.Nature 2017;548:537–42. https://doi.org/10.1038/nature23477
19. Singh S,Toor JS,Sharma A et al. Signature genes associated with immunological non responsiveness to anti-retroviral therapy in HIV-1 subtype-c infection.PLoS One 2020;15:e0234270. https://doi.org/10.1371/journal.pone.0234270
20. Qi Y,Li X,Chang C et al. Ribosomal protein L23 negatively regulates cellular apoptosis via the RPL23/Miz-1/c-Myc circuit in higher-risk myelodysplastic syndrome.Sci Rep 2017;7:2323. https://doi.org/10.1038/s41598-017-02403-x
21. Dai M-S,Zeng SX,Jin Y et al. Ribosomal protein L23 activates p53 by inhibiting MDM2 function in response to ribosomal perturbation but not to translation inhibition.Mol Cell Biol 2004;24:7654–68. https://doi.org/10.1128/MCB.24.17.7654-7668.2004
22. Gomez-Eerland R,Nuijen B,Heemskerk B et al. Manufacture of gene-modified human T-cells with a memory stem/central memory phenotype.Hum Gene Ther Methods 2014;25:277–87. https://doi.org/10.1089/hgtb.2014.004
23. Silva J,Alkan F,Ramalho S et al. Ribosome impairment regulates intestinal stem cell identity via ZAKα activation.Nat Commun 2022;13:4492.https://doi.org/10.1038/s41467-022-32220-4
24. Link AJ,LaBaer J.Trichloroacetic acid (TCA) precipitation of proteins.Cold Spring Harb Protoc 2011;2011:993–4 https://doi.org/10.1101/pdb.prot5651
25. Jersie-Christensen RR,Sultan A,Olsen JV.Phospho-proteomics, methods and protocols.Methods Mol Biol 2015;1355:251–60.
26. Demichev V,Messner CB,Vernardis SI et al. DIA-NN: neural networks and interference correction enable deep proteome coverage in high throughput.Nat Methods 2020;17:41–4. https://doi.org/10.1038/s41592-019-0638-x
27. Tyanova S,Temu T,Sinitcyn P et al. The Perseus computational platform for comprehensive analysis of (prote)omics data.Nat Methods 2016;13:731–40.https://doi.org/10.1038/nmeth.3901
28. Cox J,Mann M.MaxQuant enables high peptide identification rates,individualized p.p.b.-range mass accuracies and proteome-wide protein quantification.Nat Biotechnol 2008;26:1367–72.https://doi.org/10.1038/nbt.1511
29. Chong C,Marino F,Pak H et al. High-throughput and sensitive immunopeptidomics platform reveals profound interferonγ-mediated remodeling of the Human leukocyte antigen (HLA) ligandome*.Mol Cell Proteomics 2018;17:533–48. https://doi.org/10.1074/mcp.TIR117.000383
30. Burrows SR,Rossjohn J,McCluskey J.Have we cut ourselves too short in mapping CTL epitopes? Trends Immunol 2006;27:11–6. https://doi.org/10.1016/j.it.2005.11.001
31. Hassan C,Chabrol E,Jahn L et al. Naturally processed non-canonical HLA-A*02:01 presented peptides*.J Biol Chem 2015;290:2593–603.https://doi.org/10.1074/jbc.M114.607028
32. O'Donnell TJ,Rubinsteyn A,Laserson U.MHCflurry 2.0: improved pan-allele prediction of MHC class I-presented peptides by incorporating antigen processing.Cell Syst 2020;11:42–8.

33. Rasmussen M,Fenoy E,Harndahl M et al. Pan-specific prediction of peptide–MHC class I complex stability,a correlate of T cell immunogenicity.J Immunol 2016;197:1517–24. https://doi.org/10.4049/jimmunol.1600582
34. Nguyen AT,Szeto C,Gras S.The pockets guide to HLA class I molecules.Biochem Soc Trans 2021;49:2319–31. https://doi.org/10.1042/BST20210410
35. Wagih O.ggseqlogo: a versatile R package for drawing sequence logos.Bioinformatics 2017;33:3645–7. https://doi.org/10.1093/bioinformatics/btx469
36. Argüello RJ,Rodrigues CR,Gatti E et al. Protein synthesis regulation,a pillar of strength for innate immunity? Curr Opin Immunol 2015;32:28–35. https://doi.org/10.1016/j.coi.2014.12.001
37. Hart T,Chandrashekhar M,Aregger M et al. High-resolution CRISPR screens reveal fitness genes and genotype-specific cancer liabilities.Cell 2015;163:1515–26. https://doi.org/10.1016/j.cell.2015.11.015
38. Harndahl M,Rasmussen M,Roder G et al. Peptide–MHC class I stability is a better predictor than peptide affinity of CTL immunogenicity.Eur J Immunol 2012;42:1405–16. https://doi.org/10.1002/eji.201141774
39. Burg SHvd,Visseren MJ,Brandt RM et al. Immunogenicity of peptides bound to MHC class I molecules depends on the MHC–peptide complex stability.J Immunol 1996;156:3308–14. https://doi.org/10.4049/jimmunol.156.9.3308
40. Chalabi M,Verschoor YL,Tan PB et al. Neoadjuvant immunotherapy in locally advanced mismatch repair–deficient colon cancer.N Engl J Med 2024;390:1949–58. https://doi.org/10.1056/NEJMoa2400634
41. Elliff J,Biswas A,Roshan P et al. Dynamic states of eIF6 and SDS variants modulate interactions with uL14 of the 60S ribosomal subunit.Nucleic Acids Res 2023;51:1803–22. https://doi.org/10.1093/nar/gkac1266
42. Zhang F,Hamanaka RB,Bobrovnikova-Marjon E et al. Ribosomal stress couples the unfolded protein response to p53-dependent cell cycle arrest*.J Biol Chem 2006;281:30036 45.https://doi.org/10.1074/jbc.M604674200
43. Zhu K,Wang J,Zhu J et al. p53 induces TAP1 and enhances the transport of MHC class I peptides.Oncogene 1999;18:7740–7. https://doi.org/10.1038/sj.onc.1203235
44. Wang B,Niu D,Lai L et al. p53 increases MHC class I expression by upregulating the endoplasmic reticulum aminopeptidase ERAP1.Nat Commun 2013;4:2359. https://doi.org/10.1038/ncomms3359

Supplementary data

Supp. Figure 1

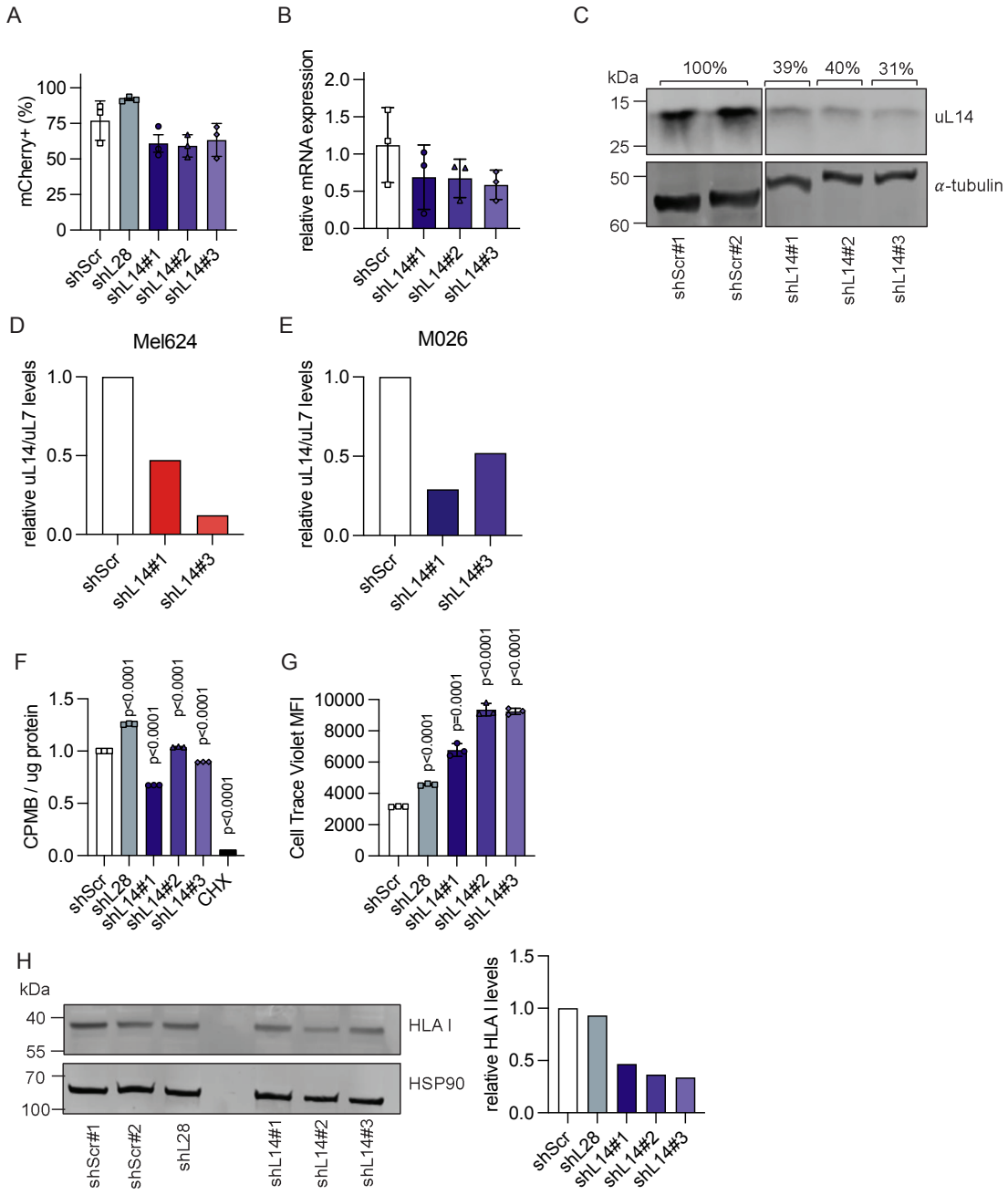

Supplemental Figure 1.

(**A**)Transduction efficiency (measured by % of cells with mCherry expression) of M026 cells was measured by flow cytometry gated on live tumor cells. n=3 independent experiments each assessed in triplicates represented as mean ± SEM.

(**B**) RT-qPCR analysis confirming efficient uL14 KD in M026 tumor cells. ACTB was used as a reference. n=3 technical replicates represented as mean ± SD. p values were calculated using a two-tailed t-test.

(**C**) Western blot analysis confirming efficient uL14 KD in M026 tumor cells. α-tubulin was used as loading control. n=1 experiment per cell line.
(**D**) Quantification of Western blot analysis confirming in Mel624 cells that uL14 KD results in decreased uL14 incorporation in the ribosome. Quantification is relative to uL7. n=1 experiment.
(**E**) Quantification of Western blot analysis confirming in M026 cells that uL14 KD results in decreased uL14 incorporation in the ribosome. Quantification is relative to uL7. n=1 experiment.
(**F**) 35S-methionine incorporation assay showing decreased protein synthesis in shL14 M026 tumor cells compared to the control. Cycloheximide (CHX) was used as a control to inhibit protein synthesis. n=3 technical replicates represented as mean ± SD. P values were calculated using a two-tailed t-test.
(**G**) CellTrace violet cell proliferation assay showing decreased cell proliferation in shL14 M026 cells compared to control cells. Proliferation was assessed by flow cytometry using the MFI. n=3 biological replicates represented as mean ± SEM. p values were calculated using a two-tailed t-test.
(**H**) Western blot showing decreased HLA I protein levels in shL14 M026 tumor cells compared to the control. HSP90 was used as loading control. n=1 independent experiment.

Supp. Figure 2

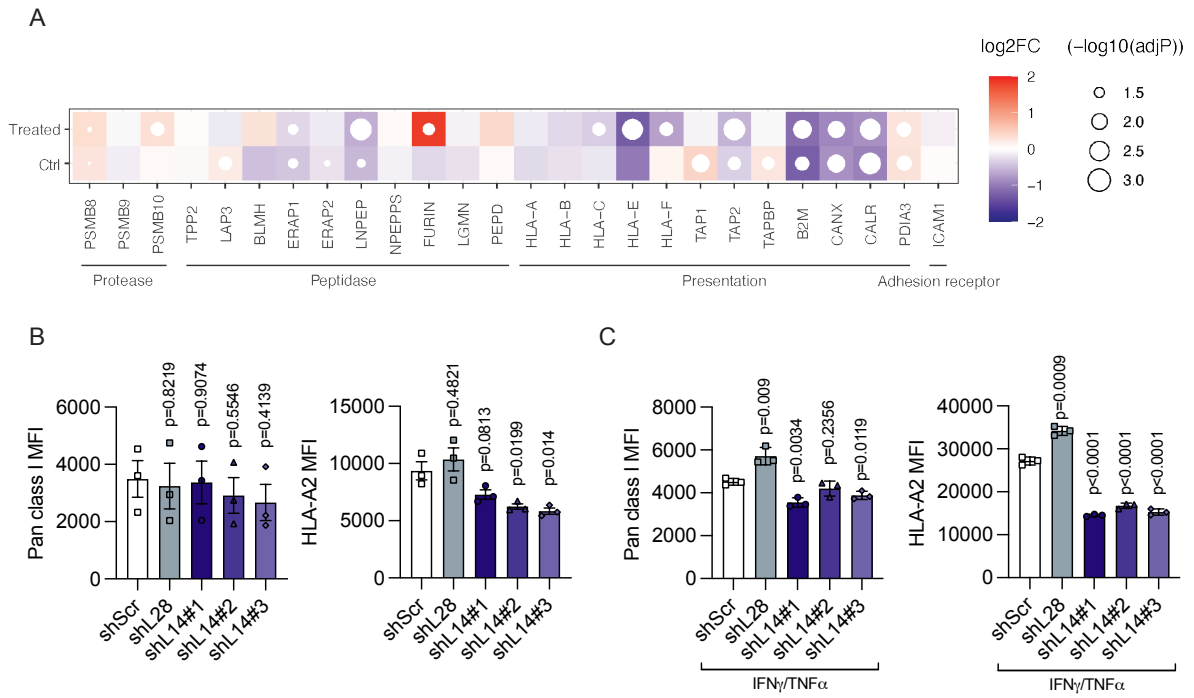

Supplemental Figure 2.

(**A**) Proteomics analysis of M026 cells reveals altered protein levels upon uL14 KD in untreated (Ctrl) cells and cells treated with IFNγ/TNFα (Treated). n=3 independent experiments, and *p* values were calculated using a two-tailed t test.

(**B**) uL14 KD decreases HLA I surface levels in M026 tumor cells. HLA surface levels were measured by flow cytometry using the MFI. n=3 independent experiments each assessed in triplicates. Data are represented as mean ± SEM and p values were calculated using a two-tailed t test.

(**C**) uL14 KD results in low basal HLA I surface levels in M026 tumor cells treated with IFNγ/TNFα compared to the control. n=3 independent experiments each assessed in triplicates. Data are represented as mean ± SEM and p values were calculated using a two-tailed t test.

Supp. Figure 3

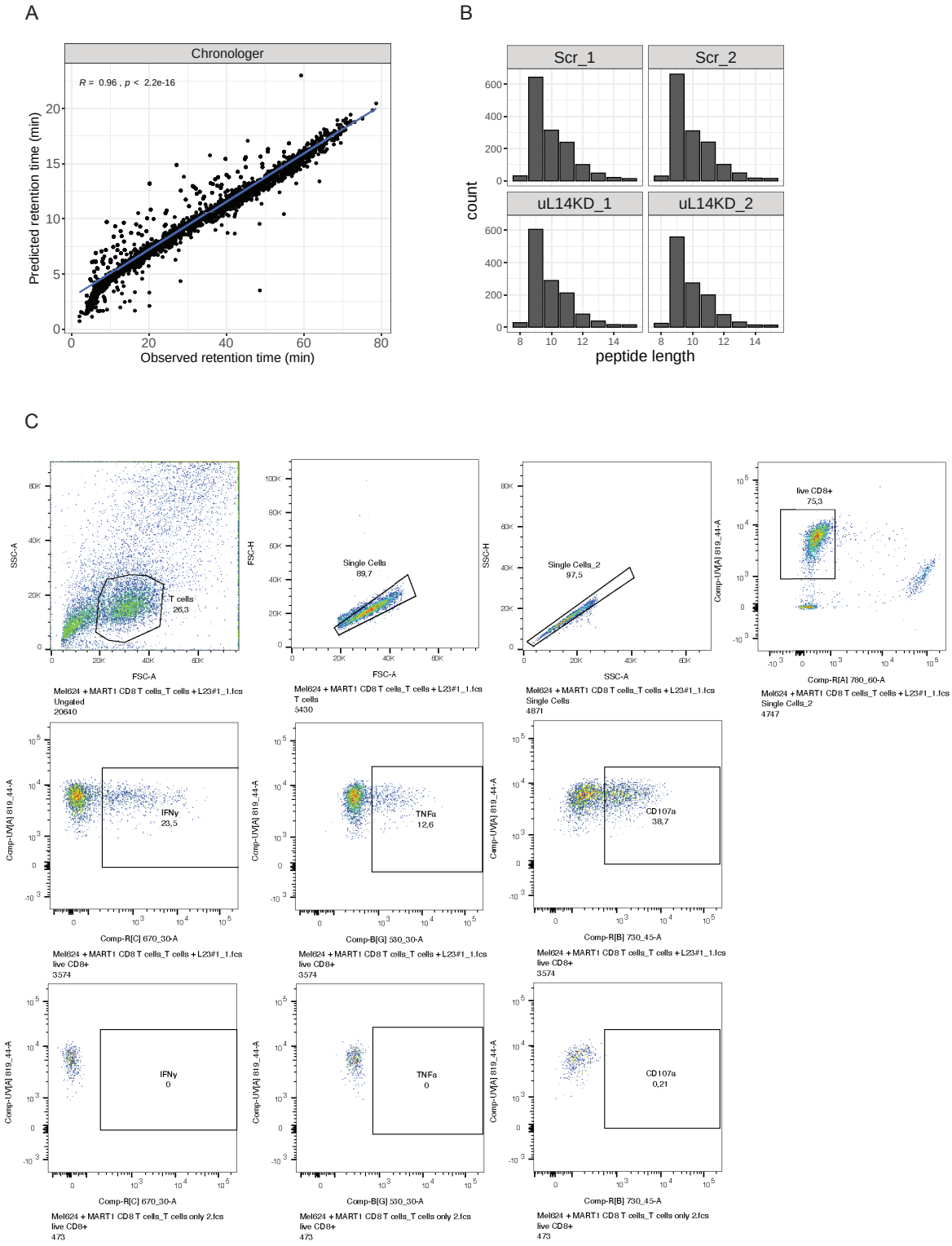

Supplemental Figure 3.

(**A**) High correlation between predicted and observed peptide retention time (min). Each point represents the predicted and observed retention time (min) for each of the identified peptides. The blue line represents a linear regression of predicted retention times for each observed retention time.

(**B**) Peptide length distribution of unique peptides identified in the shScr control and uL14 KD replicates. Each bar represents the number of peptides for a specific peptide length.
(**C**) Representation of co-culture gating strategy.

Supp. Figure 4

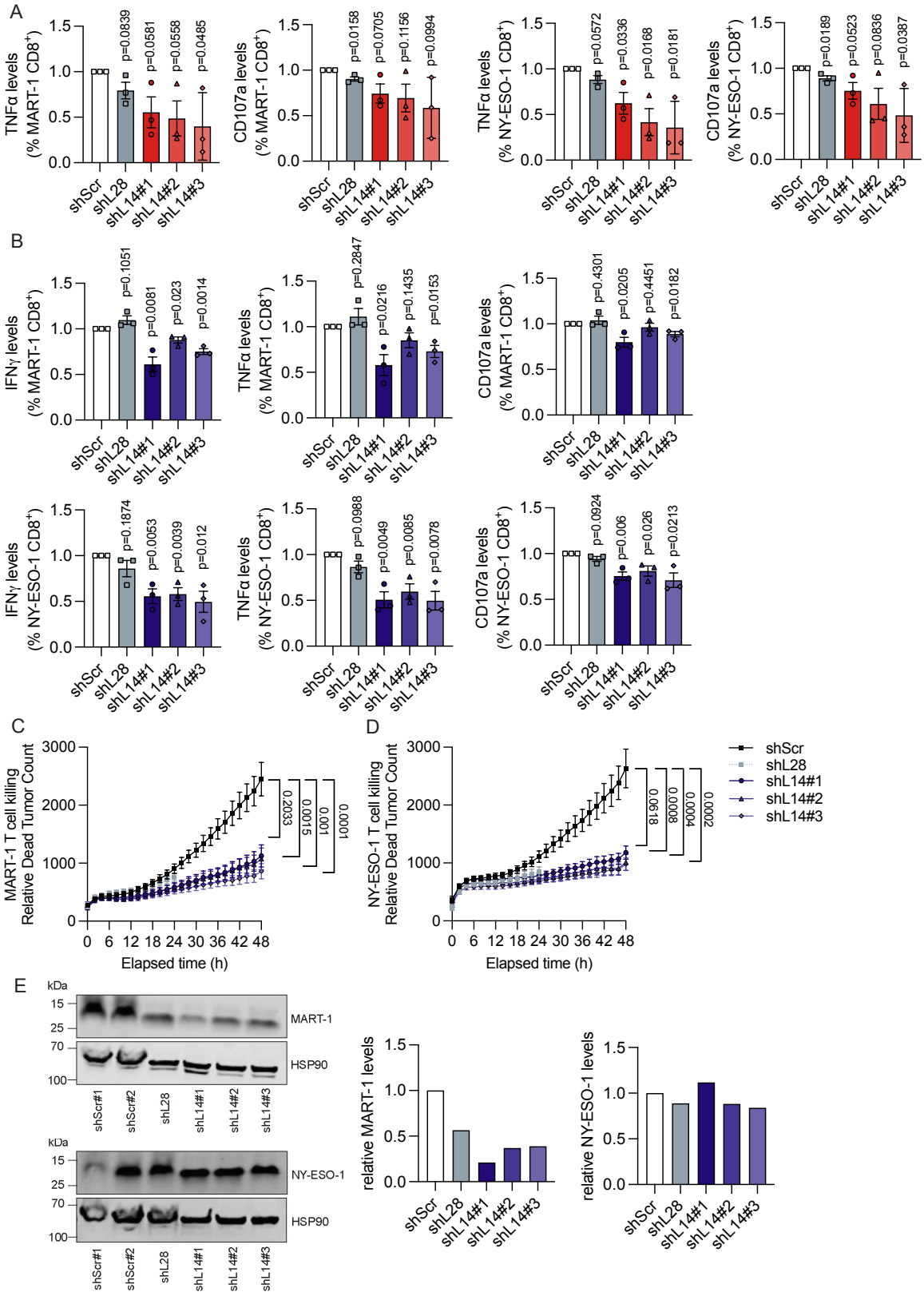

Supplemental Figure 4. [legend on the next page]

Supplemental Figure 4 [previous page].

(**A**) MART-1 and NY-ESO-1-specific $CD8^+$ T cell recognition (TNFα and CD107a levels) is decreased in shL14 Mel624 tumor cells compared to the control. n=3 independent experiments each assessed in triplicates. Data are represented as mean ± SEM and p values relative to shScrl were calculated using a two-tailed t-test.

(**B**) MART-1 and NY-ESO-1-specific $CD8^+$ T cell recognition (IFNγ,TNFα and CD107a levels) is decreased in shL14 M026 tumor cells compared to the control. n=3 independent experiments each assessed in triplicates. Data are represented as mean ± SEM and p values relative to shScrl were calculated using a two-tailed t-test.

(**C**) MART-1 specific T cell killing is suppressed in shL14 M026 tumor cells compared to shScr tumor cells. n=3 independent experiments per cell line, each assessed in triplicates. Data represent mean and error ± SEM and p values were calculated with a two-tailed t-test.

(**D**) NY-ESO-1 specific T cell killing is suppressed in shL14 M026 tumor cells compared to shScr tumor cells. n=3 independent experiments per cell line, each assessed in triplicates. Data represent mean and error ± SEM and p values were calculated with a two-tailed t-test.

(**E**) Western blot showing decreased MART-1 and NY-ESO-1 source protein levels in shL14 M026 tumor cells compared to the shScr control. HSP90 was used as loading control. n=1 experiment per cell line.